PERGAMON

International Journal of Solids and Structures 38 (2001) 4071–4089

INTERNATIONAL JOURNAL OF SOLIDS and STRUCTURES

www.elsevier.com/locate/ijsolstr

A dynamic buckling geometric approach of 2-DOF autonomous potential lumped-mass systems under impact loading

C.J. Gantes [a,*], A.N. Kounadis [a], J. Raftoyiannis [a], V.V. Bolotin [b]

[a] *Laboratory of metal structures, Department of Civil Engineering, National Technical University of Athens, P.O. Box 31830, 100-35 Athens, Greece*

[b] *Laboratory of Reliability, Institute of Mechanical Engineering Research, Russian Academy of Sciences, 4M Kharitonyevsky Lane, 101830 Moscow, Russia*

Received 19 February 1999

Abstract

Dynamic buckling for autonomous nondissipative lumped-mass systems under impact loading is thoroughly investigated. It is assumed that a fully plastic impact due to a striking body falling freely from a given height takes place, and that the effect of wave propagation can be neglected. Attention is focused on the post-impact dynamic buckling after establishing the initial velocities and the associated initial kinetic energy. Via a thorough discussion of the dynamic buckling mechanism based on certain salient geometric features of the total potential energy surface, one can obtain practically ''exact'' dynamic buckling loads, by extending previous findings valid for step load of infinite duration to the case of impact load. The proposed geometric approach, which is described for n-DOF systems and then presented in detail for 2-DOF systems, gives comprehensive, direct, readily obtained and reliable solutions compared to numerical integration schemes. © 2001 Elsevier Science Ltd. All rights reserved.

Keywords: Dynamic buckling; Impact; Energy; Approximation

1. Introduction

The field of nonlinear stability of structures which has gained particular importance long time ago (Bolotin, 1964) continues in our days to attract the interest of researchers (Simitses, 1989), in view also of the recent progress in nonlinear dynamics and chaos (Thompson and Stewart, 1986). Nonlinear dynamic buckling of dissipative/nondissipative discrete systems under step constant directional (conservative) loading of infinite, finite or very short duration as well as pertinent criteria for establishing approximate and lower/upper bound dynamic buckling estimates have been critically presented in various studies (Kounadis,

* Corresponding author. Fax: +30-1-7723442.
E-mail address: chgantes@central.ntua.gr (C.J. Gantes).

0020-7683/01/$ - see front matter
PII: S0020-7683(00)00254-7

1991a, 1993, 1994; Kalathas and Kounadis, 1991, Gantes and Kounadis, 1995). An a priori prediction of the degree of accuracy of the dynamic buckling load (DBL) associated with zero total potential energy for autonomous nondissipative 2 or 3-DOF systems with simple (Kounadis, 1996a,b; Kounadis et al., 1999) or multiple (Kounadis and Raftoyiannis, 1997) critical points was recently presented. This is based on the geometry of the motion channel and the position of the starting point of motion relatively to the location of the stable and corresponding unstable (saddle) equilibrium point, via the neighbourhood of which the escaped motion (dynamic buckling) takes place. Thus, a geometric approach based on certain salient features of the zero level total potential energy "surface" or "hypersurface" (for n-DOF systems with $n \geqslant 3$) in conjunction with the total energy-balance equation allow establishment of new stability criteria (Kounadis, 1999a) leading to readily obtained, practically "exact", DBLs for autonomous nondissipative systems.

A major difficulty for establishing the response of such autonomous potential systems is that quite often one has to overcome numerical difficulties associated with the long term response (Kounadis, 1991b) (related to dynamic buckling), behaviours very sensitive to initial conditions (Kalathas and Kounadis, 1991), or to damping (Kounadis, 1991b), as well as cases with alternative narrow regions of stability/instability as the loading increases slowly from zero (Kalathas and Kounadis, 1991). Additional difficulties arise when numerical schemes are applied to the case of dynamic buckling impact analysis since the initial conditions are unknown. These drawbacks become more acute when a multi-parameter discussion is required.

In view of the above, modern computational techniques slide gradually away from the classical integration schemes, perturbation and averaging techniques, being steadily oriented to more sophisticated methods based on energy, topological and geometrical concepts together with a profound knowledge of the physical phenomena related to the pertinent problem. The powerful techniques of the center manifold theorem (Carr, 1981) and of Lyapunov–Schmidt (Chow and Hale, 1982) for reducing the system dimension are local in character and need the transformation of the field equations into a standard form, difficult, in general, to be established. Hence, exact DBLs of general discrete systems can be determined only through a global (nonlinear) dynamic analysis associated with several drawbacks mentioned above. Nevertheless, one can obtain practically "exact" DBLs by the aforementioned geometric approach, employed for n-DOF systems which under statically applied load experience either a limit point instability (Fig. 1a) or an unstable branching point instability bifurcating from a nonlinear prebuckling path (Fig. 1b). The main objective of this analysis is to extend the above powerful geometric approach (Kounadis, 1999a), valid for dynamic buckling under step loading, to the case of dynamic buckling under impact loading.

A simple dynamic buckling problem of a 2-DOF lumped-mass cantilever model under impact loading based on lower bound dynamic buckling estimates was presented by Kounadis (1993). Fully plastic impact (Goldsmith, 1960) via a heavy body falling freely from a given height (Kounadis, 1982), which strikes centrally the tip-mass, was postulated. It was also assumed that the height was sufficiently small (compared with the height of the cantilever) and that the ratio of masses is such that the effect of wave propagation can be neglected. A major step for the subsequent analysis was the determination of the initial velocities (immediately after impact) and the associated initial kinetic energy. This was accomplished by applying the law of impulse momentum together with vectorial kinematic relations among the velocities of the concentrated masses. The 2-DOF cantilever model under static loading exhibits the nonlinear equilibrium path of Fig. 1a, while the model of a simply supported column (Kounadis, 1991a) the nonlinear equilibrium path of Fig. 1b. Recently the impact analysis of the 2-DOF model was extended to an n-DOF lumped-mass cantilever model (Kounadis et al., 1997). In the present work, the degree of accuracy of the results of the above approximate impact analyses will be checked via the aforementioned geometric approach (Kounadis, 1996a,b, 1999) as extended and refined in a recent work (Gantes et al., 1998), and subsequently via the numerical scheme of Runge–Kutta. The theoretical treatment of the problem will be presented for multi-DOF systems, even though numerical results will be restricted to 2-DOF systems.

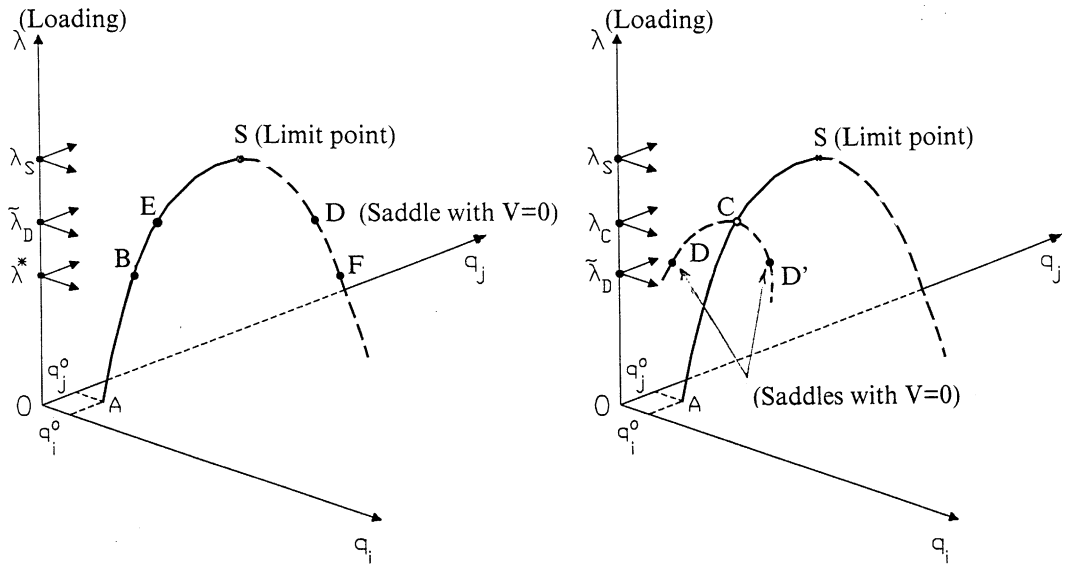

Fig. 1. Nonlinear equilibrium paths (λ versus q_i and q_j): (a) of a typical limit point system and (b) of an unstable bifurcational system.

2. Statement of the problem

Consider the n-DOF cantilever model with concentrated masses shown in Fig. 2 which is assumed to simulate the continuous system of a weightless cantilever beam. It consists of n weightless rigid links of equal length ℓ, interconnected to each other as well as to the ground by frictionless hinges and corresponding nonlinear torsional springs with equal linear stiffness constants k and different nonlinear (quadratic) stiffness constants δ_i $(i = 1, \ldots, n)$. The springs may be related to corresponding linear viscous dampers with coefficients c_i, thus simulating not only the stiffness properties but also the damping of the continuous beam. Weightless concentrated masses m_i $(i = 1, \ldots, n)$ simulate as lumped the distributed mass of the links attached at the hinges.

It should be mentioned that the process of discretization of the continuous beam into a discrete model is beyond the scope of our paper. Our objective is to treat a discrete model, which has already been discretized by some other procedure. Thus issues such as the accuracy of the discretization and the influence of the number of links are not dealt with here.

The unstressed configuration of the imperfect model before impact is specified by the initial angles ε_i $(i = 1, \ldots, n)$ between each link $A_{i-1}A_i$ and the vertical direction as shown in Fig. 2. The horizontal and vertical components of initial displacements $q^0_{i\mathrm{H}}$ and $q^0_{i\mathrm{V}}$ are readily determined (Kounadis et al., 1997) as functions of ε_i, while the corresponding displacements of the deformed configuration $q_{i\mathrm{H}}$ and $q_{i\mathrm{V}}$ in terms of the angles θ_i $(i = 1, \ldots, n)$ measured from the vertical direction (Fig. 3). Thus, the bending moment developed at joint i is given by (Kounadis et al., 1997, Kounadis, 1998)

$$M_i/k = \theta_i - \varepsilon_i + \delta_i(\theta_i - \varepsilon_i)^2, \quad i = 1, \ldots, n \tag{1}$$

The above n-DOF imperfect cantilever model is subjected to the following impact loading: a heavy body $m_0 g$ falling from a height H strikes centrally the tip mass m_n (see Fig. 2) with initial velocity

$$v_0 = \sqrt{2gH} \tag{2}$$

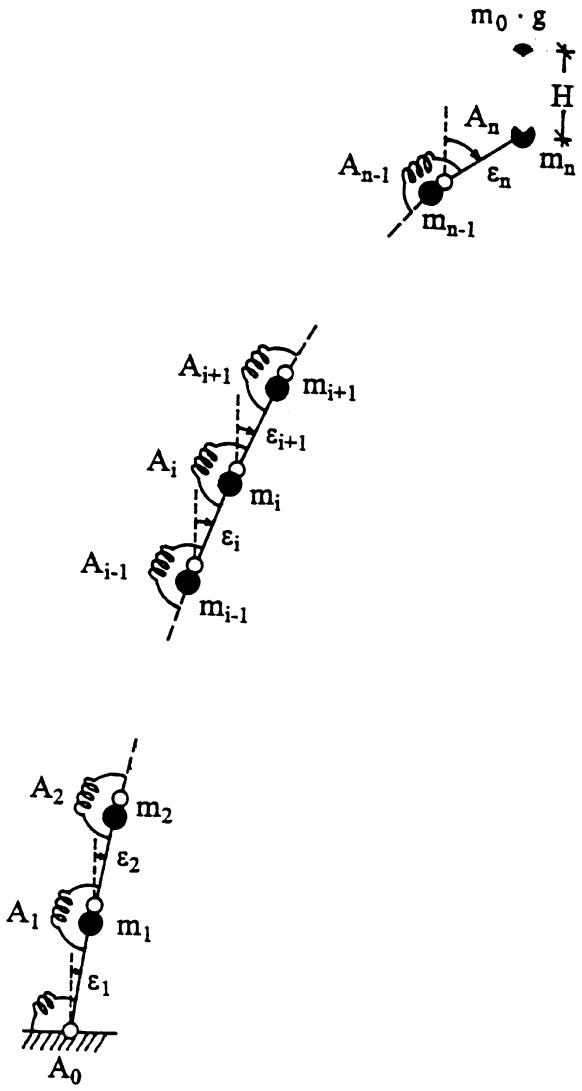

Fig. 2. Initially unstressed Ziegler's n-DOF imperfect model, before impact ($t = 0$).

where g is the gravity acceleration. The height is assumed sufficiently small (compared with the cantilever height $n\ell$) and the ratio of falling mass to system masses is such that the effect of wave propagation can be neglected. A fully plastic impact (Goldsmith, 1960) is postulated and thus, the two masses m_0 and m_n attain immediately after impact the same velocity $\mathbf{v}_n$ $(= \dot{\mathbf{q}}_n^0)$ and do not separate thereafter (Goldsmith, 1960; Kounadis, 1982). This is illustrated in Fig. 3 showing that the tip mass (immediately after impact, i.e. at time $t = 0$) is $M = m_0 + m_n$.

The magnitudes of initial $(t = 0)$ displacements $\mathbf{q}_i^0$, a priori known, can be computed in terms of $\theta_i(0)$ as follows

$$\theta_i(0) = \varepsilon_i \quad (i = 1, \ldots, n) \tag{3}$$

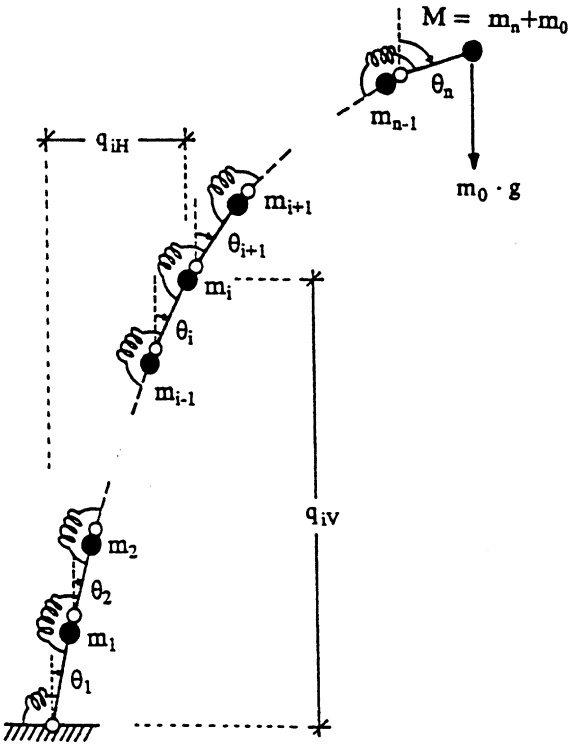

Fig. 3. Deformed configuration of n-DOF imperfect model, after impact (at $t > 0$).

Thus, one has to determine the initial velocities $\dot{\mathbf{q}}_i^0 = \dot{\mathbf{q}}_i(\varepsilon_i)$ (and thereafter the initial angular velocities $\dot{\theta}_i(0)$) of each mass m_i $(i = 1, \ldots, n)$ in terms of the impact loading $m_0 g$ and ε_i. To this end we observe the following:

At the time $t = 0$ the mass m_1 acquires a velocity $\mathbf{v}_1 (= \dot{\mathbf{q}}_1^0)$ of unknown magnitude $v_1 (= \dot{q}_1^0)$ that is perpendicular to the link A_0A_1. Masses $m_2, \ldots, m_{n-1}$ assume velocities $\mathbf{v}_2 (= \dot{\mathbf{q}}_2^0), \ldots, \mathbf{v}_{n-1} (= \dot{\mathbf{q}}_{n-1}^0)$ with unknown magnitudes and directions that can be determined using the law of impulse momentum combined with vectorial kinematic relations (Kounadis et al., 1997) among the velocities of the masses. Since the procedure for determining the initial velocities $\dot{\mathbf{q}}_i^0$ (and $\dot{\theta}_i(0)$) is described in detail by Kounadis (1993) and Kounadis et al. (1997), the present analysis will be basically confined to the post-impact response.

The initial velocities $\dot{\theta}_i(0)$ (determined analytically by Kounadis et al. (1997)) together with the initial displacements $\theta_i(0) = \varepsilon_i$ (a priori known) constitute the initial conditions of the problem. Note that the initial conditions are linear functions of two external control parameters: the striking mass m_0 (or the loading $P = m_0 g$) and the falling height H (or the initial velocity $v_0 = \sqrt{2gH}$). Hence, keeping the one control parameter constant one can find the value of the other smoothly varying parameter that will cause dynamic buckling. If $m_0 \neq 0$ (i.e. $P = m_0 g \neq 0$) and $H = 0$ the initial angular velocities vanish (i.e. $\dot{\theta}_i(0) = 0$ for all i). These angular velocities become also zero, if $H \neq 0$ but $m_0 = 0$ (i.e. $P = 0$).

It should be mentioned that the height of impact is not sufficient to determine an initial velocity and then a buckling load, unless an additional criterion is imposed. This criterion will be to seek the minimum falling mass that causes buckling for given height or the minimum height for given mass.

3. Post-impact response

The response of the system after impact subject to the previous initial conditions, can be described by the following set of Lagrange equations of motion (Kounadis, 1996a,b).

$$\frac{\mathrm{d}}{\mathrm{d}t}\left(\frac{\partial K}{\partial \dot{\theta}_i}\right) - \frac{\partial K}{\partial \theta_i} + \frac{\partial V}{\partial \theta_i} + \frac{\partial F}{\partial \dot{\theta}_i} = 0, \quad i = 1, \ldots, n \tag{4}$$

where K is the positive definite function of the total kinetic energy; $V = V(\theta_i; \lambda; \varepsilon_i)$ is the total potential energy, being a nonlinear function of $\theta_i = \theta_i(t)$ and linear function of the dimensionless loading $\lambda = P\ell/k = m_0 g\ell/k$ resulting after impact; F is a nonnegative definite dissipation function.

As stated above, dynamic buckling is governed by two external control parameters: the loading λ and the falling height $h = H/n\ell$ (from which the initial conditions are dependent). If $h = 0$ we have the case of a suddenly applied (step) load of infinite duration which can be treated very efficiently using the aforementioned geometric approach (Kounadis, 1999). A description of this approach will allow a comprehensive transition to the case of dynamic buckling due to impact.

3.1. Step load of infinite duration

For such a type of loading all initial angular velocities $\dot{\theta}_i(0)$ are zero; hence, the response of the system is governed by Eq. (4) subject to the initial conditions (3) which define the location of the starting position of motion (see point A in Fig. 1a,b) in the V-displacement space for fixed λ. The total energy E of the above autonomous system (including the loss of energy) at any time $t > 0$ for a system initially $(t = 0)$ unstressed is given by

$$E = K + V + 2\int_0^t F\mathrm{d}t' = 0 \tag{5}$$

From Eq. (5) – being the first integral of Eq. (4) – follows that throughout the motion (including dynamic buckling, being an escaped motion)

$$V(\theta_i, \lambda; \varepsilon_i) \leqslant 0 \quad (i = 1, \ldots, n) \tag{6}$$

while if $V > 0$ there is no motion, and thus dynamic buckling.

According to the stability criterion adopted herein (Kounadis, 1996a,b, 1999; Kounadis et al., 1999; Kounadis and Raftoyiannis, 1997) (boundedness of solution) dynamic buckling (in the large) is defined as that state for which an escaped motion becomes unbounded (overflow) or of very large amplitude or is captured (if damping is included) by a remote equilibrium state (acting as point attractor). The minimum load corresponding to this state is defined as the DBL. Dynamic buckling for an n-DOF cantilever model associated with the equilibrium path of Fig. 1a occurs sometimes via a saddle point D (with $V = 0$) or usually via the neighbourhood of D (with very small negative V). For systems associated with an unstable symmetric branching point (Fig. 1b) there are two saddles D and D' (with $V = 0$) as discussed by Kounadis et al. (1999) and Kounadis (1999). The DBL corresponding to $V = 0$ is denoted by $\tilde{\lambda}_{\mathrm{D}}$. In nondissipative systems $\tilde{\lambda}_{\mathrm{D}}$ coincides with the exact DBL λ_{D}, of 1-DOF systems and under certain conditions with the exact DBL λ_{D} of n-DOF systems, being in general for the latter systems a lower bound dynamic buckling estimate (Kounadis, 1996a,b), i.e. $\tilde{\lambda}_{\mathrm{D}} \leqslant \lambda_{\mathrm{D}}$.

The load $\tilde{\lambda}_{\mathrm{D}}$ and the corresponding saddles θ_i^{D} (on the unstable path) of the cantilever model under discussion are obtained for given initial conditions (3) by solving the systems of $(n + 1)$ equations (Kounadis, 1996a,b),

$$\left.\begin{matrix} V_i(\theta_i, \lambda; \varepsilon_i) = 0 \\ V(\theta_i, \lambda; \varepsilon_i) = 0 \end{matrix}\right\}, \quad i = 1, \ldots, n \tag{7}$$

The error (difference) $E = \lambda_D - \tilde{\lambda}_D$ is more conveniently determined by considering 2-DOF systems for which one has a geometric picture of the total potential energy "surface" $V(\theta_i, \lambda; \varepsilon_i)$ in the three-dimensional V-displacement space. For such a model at a fixed load $\overset{*}{\lambda} < \tilde{\lambda}_D$ the "surface" $V(\theta_i, \lambda; \varepsilon_i)$ passing through the point A (defined by the initial displacements ε_1, ε_2), the stable equilibrium B (defined by θ_1^B, θ_2^B) and the saddle F (defined by θ_1^F, θ_2^F) is shown in Fig. 4a. Points B and F correspond both to $\overset{*}{\lambda}$. At point B the total potential V is minimum, at point A we have $V = 0$, while V at the saddle F is positive.

The intersection of V with the horizontal plane $0\theta_1\theta_2$ is a plane closed curve $V = 0$ passing always through the starting point of motion A. Fig. 4b shows the projection of motion in the horizontal plane. If $\lambda < \tilde{\lambda}_D$ any motion starting from A cannot escape via the saddle $F(\theta_1^F, \theta_2^F)$ since above the horizontal plane $V > 0$, which implies no motion (and hence no dynamic buckling). However, as λ increases, the saddle F is coming down approaching the horizontal plane $0\theta_1\theta_2$. At $\lambda = \tilde{\lambda}_D$ (for which $V = 0$) the "surface" V touches this plane at the saddle D (Fig. 5a). The new closed curve $V = 0$ (intersection of the V-surface with the $0\theta_1\theta_2$-plane) passes through the points A and D. The projection E′ of the stable equilibrium (corresponding to $\tilde{\lambda}_D$) is surrounded by the plane (closed) curve $V = 0$. Since motion occurs only if $V \leqslant 0$, considering the variation of ($V \leqslant 0$) within the vertical plane passing through the equilibria E and D, we observe that V has minimum at E and maximum at D. A motion that starts from A (taking place in the interior of the surface $V \leqslant 0$) can escape through the saddle D only when the points A, E and D are located in the same vertical plane. Then, the starting point of motion A coincides with G (Fig. 5b), a fact which implies, $\tilde{\lambda}_D \equiv \lambda_D$. If this is not so (i.e. A ≠ G), the motion starting from point A cannot reach point D but will stop at a point of the line E′D where the "width" of the curve $V = 0$ (defined by distance between the two points of intersection of $V = 0$ with the normal on E′D is smaller than the "width" of this curve at point A. Then, the motion

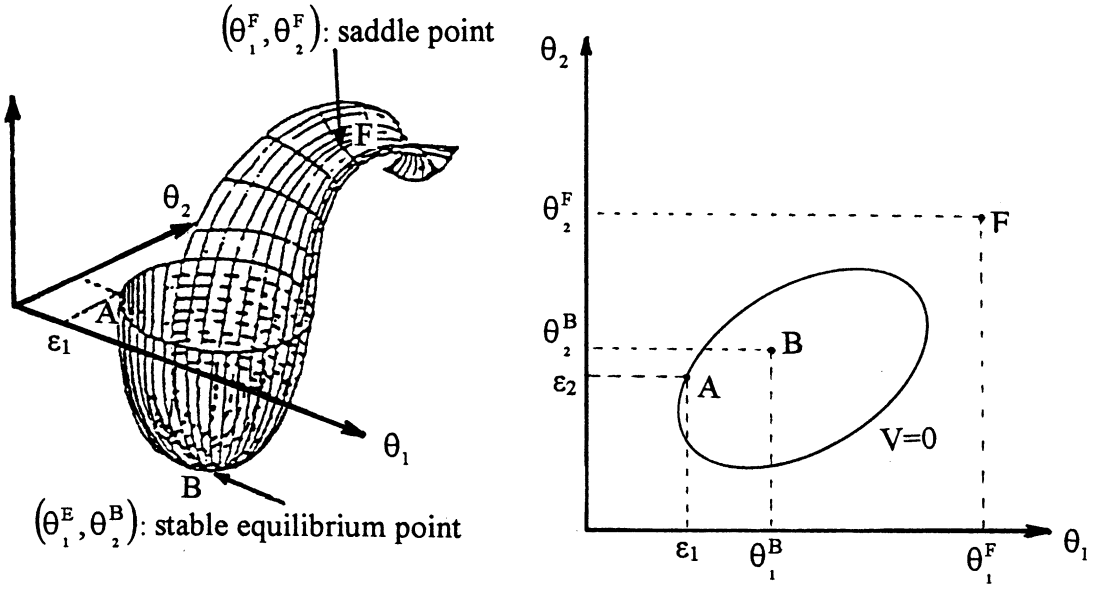

Fig. 4. (a) Energy surface V(at $\lambda^* < \tilde{\lambda}_D$) for a 2-DOF system, and (b) projection of motion on $0\theta_1\theta_2$-plane.

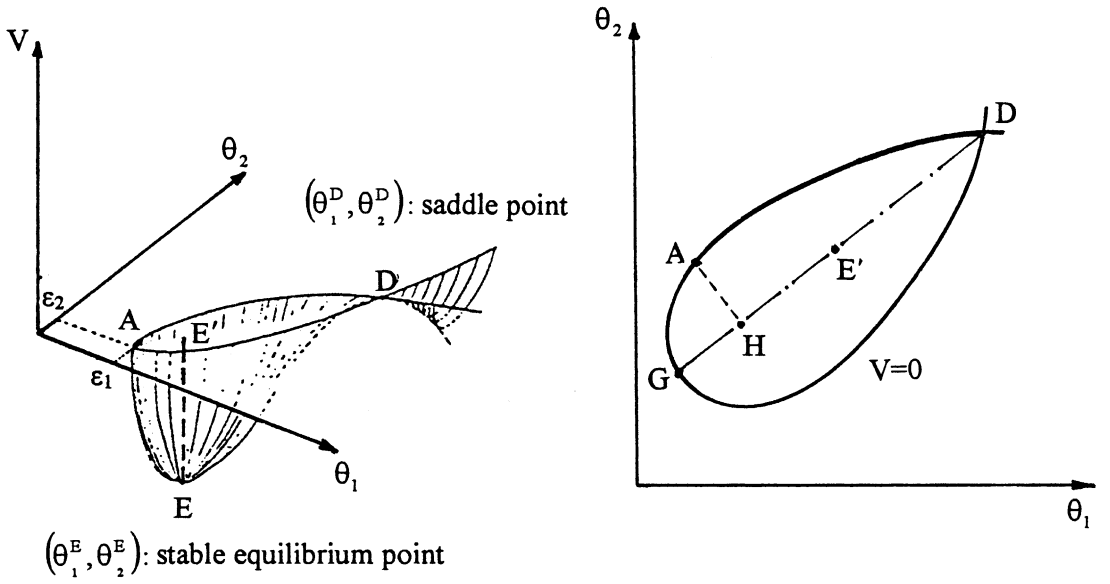

Fig. 5. (a) Total potential surface $V \leqslant 0$ at $\lambda = \tilde{\lambda}_D$, and (b) its intersection with the $0\theta_1\theta_2$-plane for a 2-DOF system.

consists of back and forth oscillations between these two points around the stable equilibrium E which is a center. As point A is going away from the vertical plane (passing through the points E and D) the difference $E = \lambda_D - \tilde{\lambda}_D$ increases (Kounadis 1996a,b, 1999). However, by slightly increasing λ (above $\tilde{\lambda}_D$) the closed curve $V = 0$ becomes an open curve exhibiting an "opening" with "width" $\Delta_1\Delta_2$ at the corresponding new saddle D′ (Fig. 6a). If such an "opening" $\Delta_1\Delta_2$ is smaller than the width (of the new curve $V = 0$) AA′ at point A (defining the initial amplitude of the motion), an escaped motion through the neighbourhood of D′ (where $V(D') < 0$) is impossible. Then, we further increase λ in such a way so that the "width" of the curve $V = 0$ at A becomes equal to the "width" of this curve at the corresponding new saddle D″ (Fig. 6b). Then, an escaped motion (and hence dynamic buckling) will occur, and the corresponding to this situation load $\bar{\lambda}_D$ is the DBL.

3.1.1. Degree of accuracy of $\tilde{\lambda}_D$ and $\bar{\lambda}_D$

The degree of accuracy of both DBLs $\tilde{\lambda}_D$ and $\bar{\lambda}_D$ depends basically on the shape of the closed curve $V = 0$, and more specifically on the ratio of the maximum "width" versus the length of the longitudinal axis DG (Fig. 5b). As this ratio decreases the degree of accuracy of $\tilde{\lambda}_D$ and $\bar{\lambda}_D$ increases appreciably. Moreover, for a given value of this ratio (i.e. for a given shape of the closed curve $V = 0$) the error in $\tilde{\lambda}_D$ depends on the location of the starting point of motion A relatively to the two points E′ (projection of the stable equilibrium point) and the saddle D (Kounadis, 1996a,b). This is quantitatively measured with the aid of the ratio (Gantes et al., 1998) $r = (AH)/(DG)$. The decrease of r implies a much smaller error in $\tilde{\lambda}_D$. A better estimate of $\tilde{\lambda}_D$ leads to a much more accurate $\bar{\lambda}_D$.

It is worth noticing that for flexurally vibrating systems in their own plane (planar systems) the aforementioned ratio of the maximum "width" versus the length (GD) is usually very small (e.g. less than 0.20), a fact that implies a good approximate DBL $\tilde{\lambda}_D$ which subsequently leads to a DBL $\bar{\lambda}_D$ approaching (i.e. $\bar{\lambda}_D \to \lambda_D$). This allows us to consider $\bar{\lambda}_D$ practically as the "exact" DBL.

The analysis that follows is based on the last assumption regarding the shape of the closed curve $V = 0$ (associated with values of the last ratio smaller than 0.20).

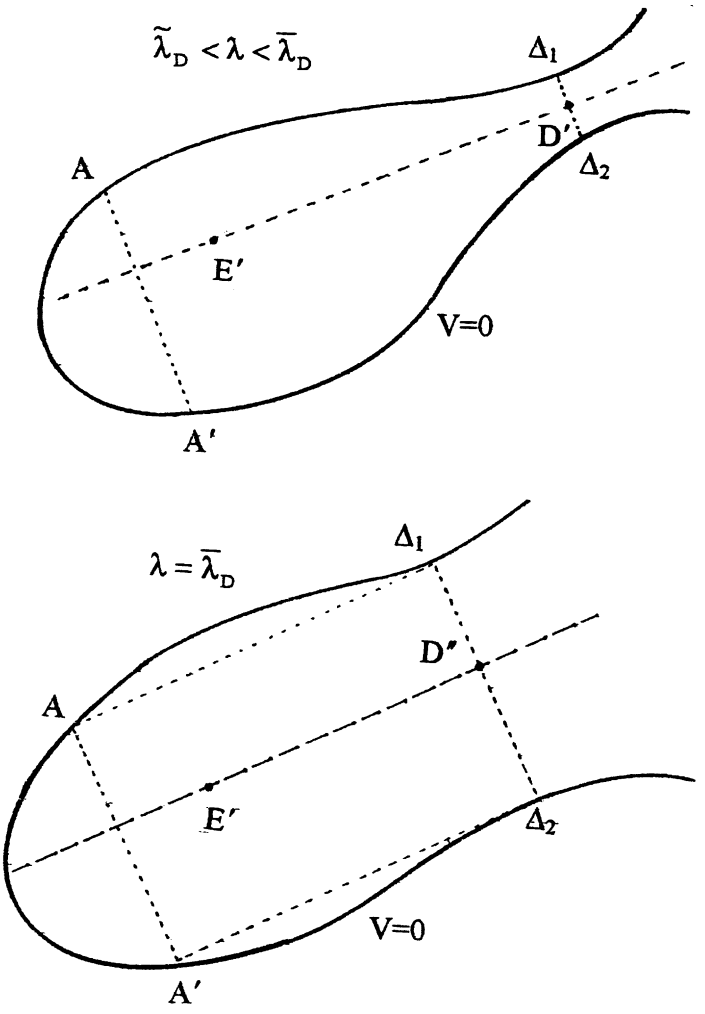

Fig. 6. Curves $V = 0$ for $\lambda > \tilde{\lambda}_D$.

3.2. Impact load

As stated above, if $H = 0$ (i.e. $v_0 = 0$) and $m_0 \neq 0$ (i.e. P or λ is different from zero), then $\dot{\theta}_i(0) = 0$ $(i = 1, \ldots, n)$. This corresponds to the previous case of a step loading of infinite duration. Now we consider the case $H \neq 0$ with $m_0 \neq 0$ (i.e. $\lambda = P\ell/k = m_0 g \ell k \neq 0$) subject to the initial conditions (3) and $\dot{\theta}_i(0) \neq 0$, where $\dot{\theta}_i(0)$ are assumed to be known or have been already determined. Comparing this case with the previous one (i.e. $H = 0$ and $m_0 \neq 0$), one should anticipate that dynamic buckling under impact load for a given height h will occur for a smaller mass m_0 than that of the step loading of infinite duration. Clearly, the magnitude of the falling mass required for dynamic buckling decreases as the height increases. Another noticeable feature of the second case is that the direction and the amplitude of the initial motion depends not only on $\theta_i(0) = \varepsilon_i$ but also on the initial angular velocities $\dot{\theta}_i(0)$. Moreover, instead of Eq. (5) the total energy E becomes

$$E = K + V + 2\int_0^t F\,\mathrm{d}t' = K^0 \tag{8}$$

where K^0 is the initial kinetic energy at time $t = 0$ evaluated by means of the known initial conditions associated with and $\dot{\theta}_i(0)$. Apparently, throughout the motion (including dynamic buckling)

$$\tilde{V} = V - K^0 \leqslant 0 \tag{9}$$

At $t = 0$ (immediately after impact) $\tilde{V} = -K^0$ since $V(t = 0) = 0$. A lower bound of the load $\tilde{\lambda}_D = m_0 g\ell/k$ (or the striking mass m_0) can be obtained by solving the system of equations

$$\left.\begin{array}{l} V_i(\theta_i;\lambda;\varepsilon_i) = 0 \\ \tilde{V}(\theta_i;\lambda;\varepsilon_i;h) = 0 \end{array}\right\} \quad (h = H/n\ell) \tag{10}$$

Following the procedure valid for the step loading we plot the curve $\tilde{V} = 0$ in the horizontal plane $0\theta_1\theta_2$ for load $\lambda = \tilde{\lambda}_D$ (see Fig. 7a). Point A from which the motion is initiated is now inside the area surrounded by the closed curve $\tilde{V} = 0$. Contrary to the previous (step loading) case this motion is associated with initial velocity. The initial direction and the corresponding maximum amplitude of motion, which are required for the subsequent analysis, depend now on both $\theta_i(0)$ and $\dot{\theta}_i(0)$. These can be established with sufficient accuracy via the linearized equations of motion. If A′ is the point of intersection of the line through A along the initial direction of motion with the curve $\tilde{V} = 0$, then AA′ (Fig. 7a) is related to the initial kinetic energy K^0. Increasing further λ (above $\tilde{\lambda}_D$), we obtain a new saddle D″ (Fig. 7b). If the "width" $\Delta_1\Delta_2$ of the new open curve $\tilde{V} = 0$ at D″ (defined above) becomes equal to the "width" A′A″ (where A″ is a point along the initial direction of motion such that A′M = MA″), then dynamic buckling occurs, otherwise we must increase the load. Point M is assumed to be associated with the minimum potential energy along the initial direction of motion. An inherent approximation is introduced via this approach and should be noted: the location of points A′ and A″ accounts fully for the value of K^0, but takes only indirectly (via the initial direction and amplitude of motion) into account the concrete values of $\dot{\theta}_1(0)$ and $\dot{\theta}_2(0)$. However, the same value of K^0 may be related to an infinite number of combinations of values of $\dot{\theta}_1(0)$ and $\dot{\theta}_2(0)$.

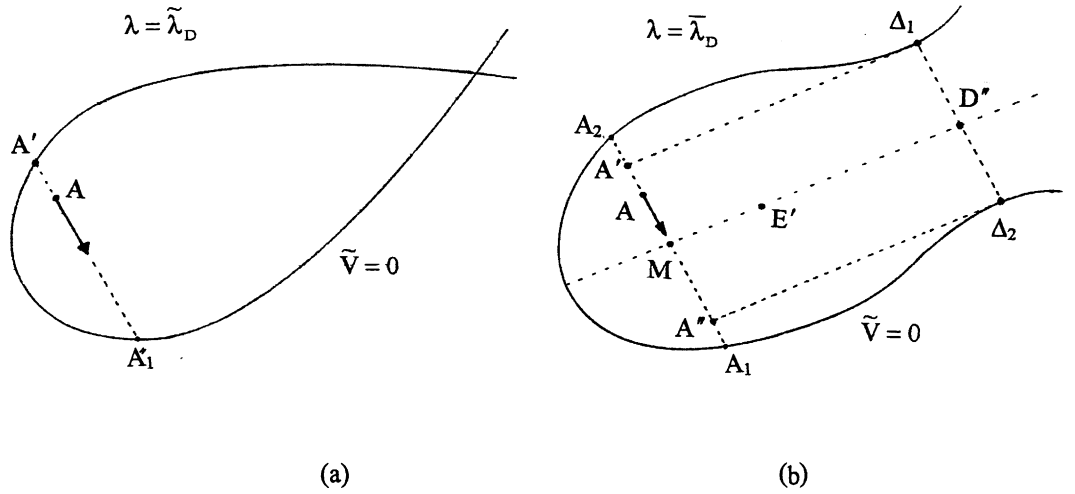

Fig. 7. Curves $\tilde{V} = 0$ for the case of impact with point A inside it (a) $\lambda = \tilde{\lambda}_D$ (b) $\lambda = \bar{\lambda}_D$.

This approximate choice of A″ was determined after an extensive numerical study and comparison to other alternatives. Theoretically, the most accurate approach is by evaluating the linearized direction of motion (see Appendix A), and then carrying out successive iterations by increasing the time until reversal of the direction of motion is detected. The point of reversal of motion is the required point A″. This approach is very demanding on computing effort and provides results which are usually negligibly better than the ones of the proposed approach. One other alternative, which is computationally simpler, is to choose point A_1'' as the point (Fig. 7a) where the line through A along the initial direction of motion intersects the curve $\tilde{V} = 0$ for $\lambda = \tilde{\lambda}_D$. This approach gives less accurate results. Another option, which is computationally cumbersome is to locate the intersections A_1 and A_2 of the line through A along the initial direction of motion with the curve $\tilde{V} = 0$ for $\lambda = \bar{\lambda}_D$ and require that $A''A_1 = A_2A'$ (Fig. 7b). This alternative gives practically the same results as the proposed method.

The equality $\Delta_1\Delta_2 = A'A''$ is readily achieved after a few trials without leading to an accumulation of error since each trial is independent of the others. The corresponding load denoted by $\bar{\lambda}_D$ is the DBL. The above analysis can be readily extended to dissipative systems (Kounadis et al., 1997).

A further question which needs clarification refers to the choice of the point in the vicinity of D″, denoted by D''_{ap}, where the "width" of the opening of the motion channel should be measured (Fig. 8). This point is located between point D″ and the point $D''_{\ell b}$, which must be defined next. D″ is the point on the static post-buckling equilibrium path for λ equal to the load we are checking. $D''_{\ell b}$ is defined as the saddle point with $V = 0$, satisfying the equilibrium equations (being constant independently of the load we are checking). Thereafter, measuring the "width" at $D''_{\ell b}$ we obtain a lower bound, $\bar{\lambda}_{D\ell b}$ of the DBL, which is a much better estimate of λ_D than $\tilde{\lambda}_D$. An even better estimate of the DBL is possible if the "width" is measured at point D''_{ap}, obtained from the equation of weighted average:

$$\frac{D''D''_{ap}}{D''D''_{\ell b}} = \frac{\bar{\lambda}_{D,\ell b}}{\bar{\lambda}_{D,\ell b} + \bar{\lambda}_{D,ap}} \tag{11}$$

where $\bar{\lambda}_{D,ap}$ is the load we are seeking. This choice yields an approximate $\bar{\lambda}_{D,ap}$ of the DBL, which is usually a better estimate than $\bar{\lambda}_{D,\ell b}$ but is no longer a lower bound, since it may be slightly larger or smaller than the exact load λ_D.

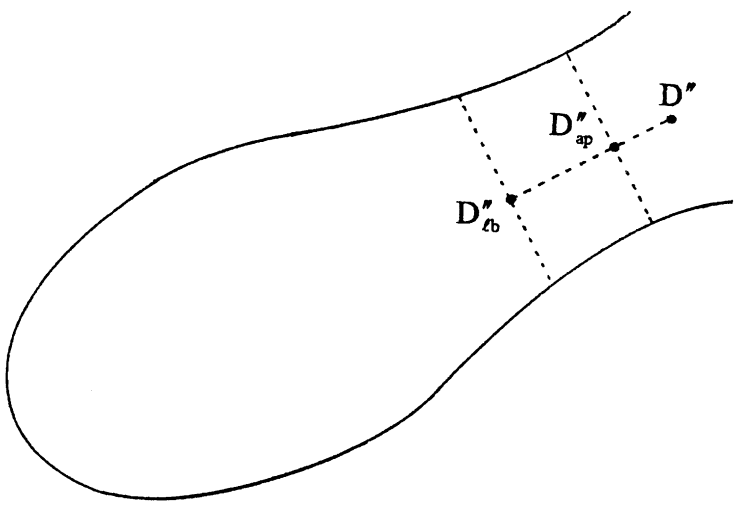

Fig. 8. Characteristic points in the vicinity of the saddle.

4. Numerical results

Consider the 2-DOF nondissipative cantilever model of Ziegler shown in Fig. 9 with initial imperfections ε_1 and ε_2, and rotational springs with quadratic stiffness components δ_1 and δ_2 for which numerical results based on $\tilde{\lambda}_D$ are available (Chow and Hale, 1982, Kounadis, 1982). For this system, the initial angular velocities $\dot{\theta}_i(0)$ $(i = 1, 2)$ are obtained by

$$\frac{\mu_1}{\mu_0\bar{v}_0}\left[\mu_1 + \sin^2(\varepsilon_2 - \varepsilon_1)\right]\dot{\theta}_1^2(0) - \left[\tfrac{1}{2}\cos\varepsilon_2\sin 2(\varepsilon_2 - \varepsilon_1) - (1+\mu_1)\cos\varepsilon_2\sin(\varepsilon_2 - \varepsilon_1) + \mu_1\sin\varepsilon_1\right]\dot{\theta}_1(0) - \mu_0\bar{v}_0\sin\varepsilon_1\cos\varepsilon_2\sin(\varepsilon_2 - \varepsilon_1) = 0$$

and

$$\dot{\theta}_2(0) = \frac{1}{\cos(\varepsilon_2 - \varepsilon_1)}\left[\mu_0\bar{v}_0\sin\varepsilon_1 - (1+\mu_1)\dot{\theta}_1(0)\right] \tag{12}$$

where $\mu_0 = m_0/(m_0 + m_2)$, $\mu_1 = m_1/(m_0 + m_2)$, $\bar{v}_0 = v_0\sqrt{(m_0 + m_2)/k}$. Taking into account that $\lambda = m_0 g\ell/k$ and $h = H/n\ell = H/2\ell$ the last expression for $\bar{v}_0$ becomes

$$\bar{v}_0 = \sqrt{2nh\lambda/\mu_0} = 2\sqrt{h\lambda/\mu_0} \tag{13}$$

For given ε_i $(i = 1, 2)$, h, μ_0 and μ_1, it follows that both $\dot{\theta}_1(0)$ and $\dot{\theta}_2(0)$ can be expressed as functions of λ. Thus, the initial kinetic energy (Chow and Hale, 1982)

$$K^0 = \tfrac{1}{2}\left[(1+\mu_1)\dot{\theta}_1^2(0) + \dot{\theta}_2^2(0) + 2\dot{\theta}_1(0)\dot{\theta}_2(0)\cos(\varepsilon_2 - \varepsilon_1)\right] \tag{14}$$

is also expressed as a function of λ. Clearly, for a given h the unknown control parameter is λ, and vice-versa. Hence, Eq. (10) can be solved with respect to θ_1, θ_2 and λ for given values of ε_i, μ_o, μ_1 and h. Since

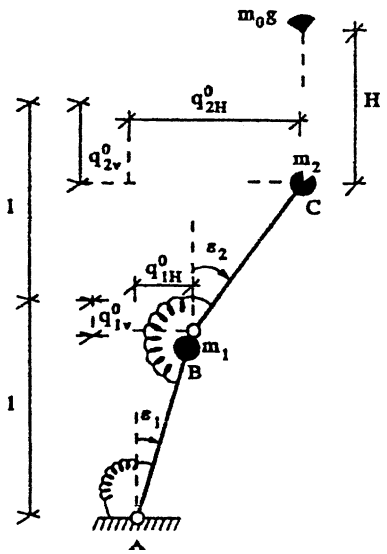

Fig. 9. 2-DOF Ziegler model.

there are two sets of values of $\dot{\theta}_1(0)$ and $\dot{\theta}_2(0)$ obtained from Eq. (12), Eq. (10) also gives two corresponding values of $\lambda = \tilde{\lambda}_D$, the minimum of which is a lower bound of the exact DBL.

It should be noted that although the DBL λ_D is related to the mass m_0, the initial-value problem is properly defined, if in addition to the ratio m_1/m_2, the ratio m_0/m_1 (or m_0/m_2) is a priori know. This is so, because the response of the system depends not only on the ratio m_1/m_2 but also on the relative magnitude of m_0 compared to m_1 (or m_2). It is also worth noticing that one could keep constant the mass m_0 and solve with respect to h. However, such a case, requiring also a suitable reformulation of the problem regarding the choice of parameters involved, is less convenient than the first case mentioned above which is considered in the examples that follow.

If all the above assumptions are satisfied, including the last one regarding the shape of the curve $\tilde{V} = 0$ for a given 2-DOF cantilever (i.e. for given values of the parameters ℓ, k and m_1/m_2), one can proceed to the dynamic buckling analysis under impact due to a heavy body $m_0 g$ falling from a height h, as follows. For a given height h and mass ratio m_0/m_1 (or m_0/m_2) or more conveniently for given ratios μ_0 and μ_1, one can establish the DBL $\bar{\lambda}_D$ (or $m_0 = k\lambda_D/g\ell$) by applying a procedure consisting of the following steps.

First step: Obtain from Eq. (12) the angular velocities $\dot{\theta}_1(0)$ and $\dot{\theta}_2(0)$ as functions of $\bar{v}_0$ or λ using Eq. (13).
Second step: Establish via Eq. (14) K^0 as function of λ.
Third step: Solve the system of Eq. (10) from which we get $\tilde{\lambda}_D$, the saddle D and the corresponding closed curve $\tilde{V} = 0$ from the shape of which one can have a first estimate of the expected degree of accuracy of $\tilde{\lambda}_D$ and thereafter of $\bar{\lambda}_D$.
Fourth step: Increase slightly λ, evaluate the *new* (open) curve $\tilde{V} = 0$ and then from the equilibrium equations $V_1 = V_2 = 0$ the stable and unstable (saddle) points E′ and D″ corresponding to the increased λ.
Fifth step: Compute the initial direction of motion and the corresponding maximum amplitude via a linearized analysis, outlined in Appendix A and then compare the width A′A″ with the "opening" $\Delta_1\Delta_2$ of the open curve $\tilde{V} = 0$ at the saddle D″ (Fig. 8b). The load is increased until A′A″ $= \Delta_1\Delta_2$, in which case $\lambda = \bar{\lambda}_{D,\ell b}$ or $\lambda = \bar{\lambda}_{D,ap}$, depending on where the width $\Delta_1\Delta_2$ is measured.

Numerical results are given below for three different cases. The approximate buckling loads are obtained by the proposed herein analysis and then are compared with the corresponding loads $\lambda_{D,RK}$ obtained by a modified Runge–Kutta numerical integration scheme which, however, is very time-consuming, requiring successive iterations, since the initial velocities are unknown. For each problem the results are given in two columns corresponding to the two solutions of the quadratic equation for the initial conditions. Critical is the solution which gives the smaller value for the load. This value is denoted as $\bar{\lambda}^*_{D,ap}$.

First case: $\varepsilon_1 = 0.05$, $\varepsilon_2 = -0.031$, $\delta_1 = -2.5$, $\delta_2 = -0.75$, $\lambda_s = 0.360813$, $\mu_1 = 1.84$, $\mu_0 = 0.08$, $h = 1$

	First solution		Second solution	
$\lambda_{D,RK}$	0.349673		0.343117	
$\tilde{\lambda}_D$	0.305121	−12.741%	0.318938	−7.047%
$\bar{\lambda}_{D,\ell b}$	0.339831	−2.814%	0.339824	−0.960%
$\bar{\lambda}_{D,ap}$	0.346455	−0.920%	0.344546	0.417%
$\bar{\lambda}^*_{D,ap}$			0.344546	

Fig. 10 shows projections of the motion on the $\theta_1\theta_2$ plane and the corresponding curves $\tilde{V} = 0$ for this case.

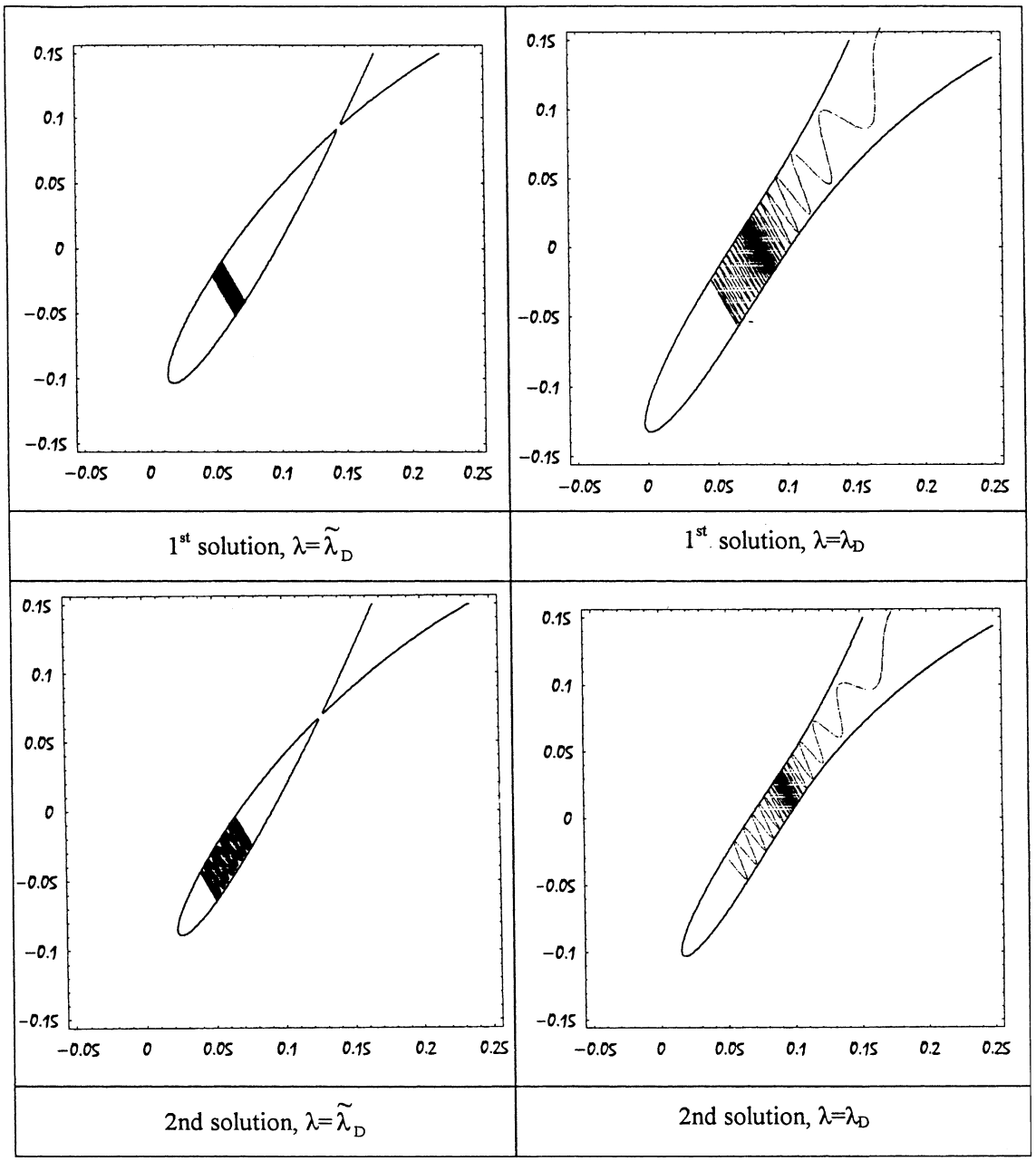

Fig. 10. Curve $\tilde{V} = 0$ and projection of motion for a 2-DOF Ziegler model with $\varepsilon_1 = 0.05$, $\varepsilon_2 = -0.031$, $\delta_1 = -2.5$, $\delta_2 = -0.75$, $\mu_1 = 1.84$, $\mu_0 = 0.08$, $h = 1$.

Second case: $\varepsilon_1 = 0.05$, $\varepsilon_2 = 0$, $\delta_1 = -2.5$, $\delta_2 = -0.75$, $\lambda_s = 0.267713$, $\mu_1 = 1.8$, $\mu_0 = 0.1$, $h = 1.6$

	First solution		Second solution	
$\lambda_{D,RK}$	0.251500		0.251497	
$\tilde{\lambda}_D$	0.248455	−1.211%	0.248465	−1.206%
$\bar{\lambda}_{D,\ell b}$	0.249878	−0.645%	0.249880	−0.643%
$\bar{\lambda}_{D,ap}$	0.249937	−0.621%	0.249940	0.619%
$\bar{\lambda}^*_{D,ap}$	0.249937			

Fig. 11 shows projections of the motion on the $\theta_1\theta_2$ plane and the corresponding curves $\tilde{V} = 0$ for this case.

Third case: $\varepsilon_1 = 0.04$, $\varepsilon_2 = -0.02$, $\delta_1 = -2$, $\delta_2 = -1$, $\mu_1 = 2$, $\mu_0 = 0.05$, $h = 1.6$

	First solution		Second solution	
$\lambda_{D,RK}$	0.326029		0.325368	
$\tilde{\lambda}_D$	0.319248	−2.080%	0.314780	−3.254%
$\bar{\lambda}_{D,\ell b}$	0.324724	−0.400%	0.323897	−0.452%
$\bar{\lambda}_{D,ap}$	0.324844	−0.363%	0.324001	0.420%
$\bar{\lambda}^*_{D,ap}$			0.324001	

The next example, shown in Fig. 12, illustrates a case where the proposed approach is not expected to give reliable results due to a "width" to length ratio of the curve $\tilde{V} = 0$ much larger than the lower bound defined in Section 3.1.1. In addition, for this case the "width" of the curve $\tilde{V} = 0$ at point D″ in the initial direction of motion changes very rapidly with increasing load. Therefore, convergence of the proposed approach encounters difficulties and the results are unsatisfactory.

In conclusion, two final comments should be made. The first is that it is possible to extend the conclusions from 2-DOF systems to *n*-DOF systems by replacing planes by hyper-planes and spaces by hyper-spaces. Such extension has been demonstrated in previous work (Kounadis et al., 1997) for the case of estimating the dynamic buckling load of systems under impact loading as well as for the case of applying geometric criteria on the energy surface, but for step loads of infinite duration (Kounadis, 1999; Gantes et al., 1998).

The second concluding comment has to do with the applicability of the proposed approach for actual engineering problems. Regarding such applications of dynamic response due to the discussed type of impact loading, one should mention simple structures that can be simulated by pertinent models, which are frequently encountered in practice, such as cranes (Kounadis, 1982). Other examples include cantilever-type vertical structures such as steel latticed towers, used for example for telecommunication applications or for elevated water tanks. The case of impact load can arise either due to the nature of operation of the structure or because of accidents, for example in case of objects falling from moving cranes.

Acknowledgements

This work has been funded partially by the International Association for the promotion of cooperation with scientists from the New Independent States of the former Soviet Union through project INTAS-RFBR 95-0433. This support is gratefully acknowledged.

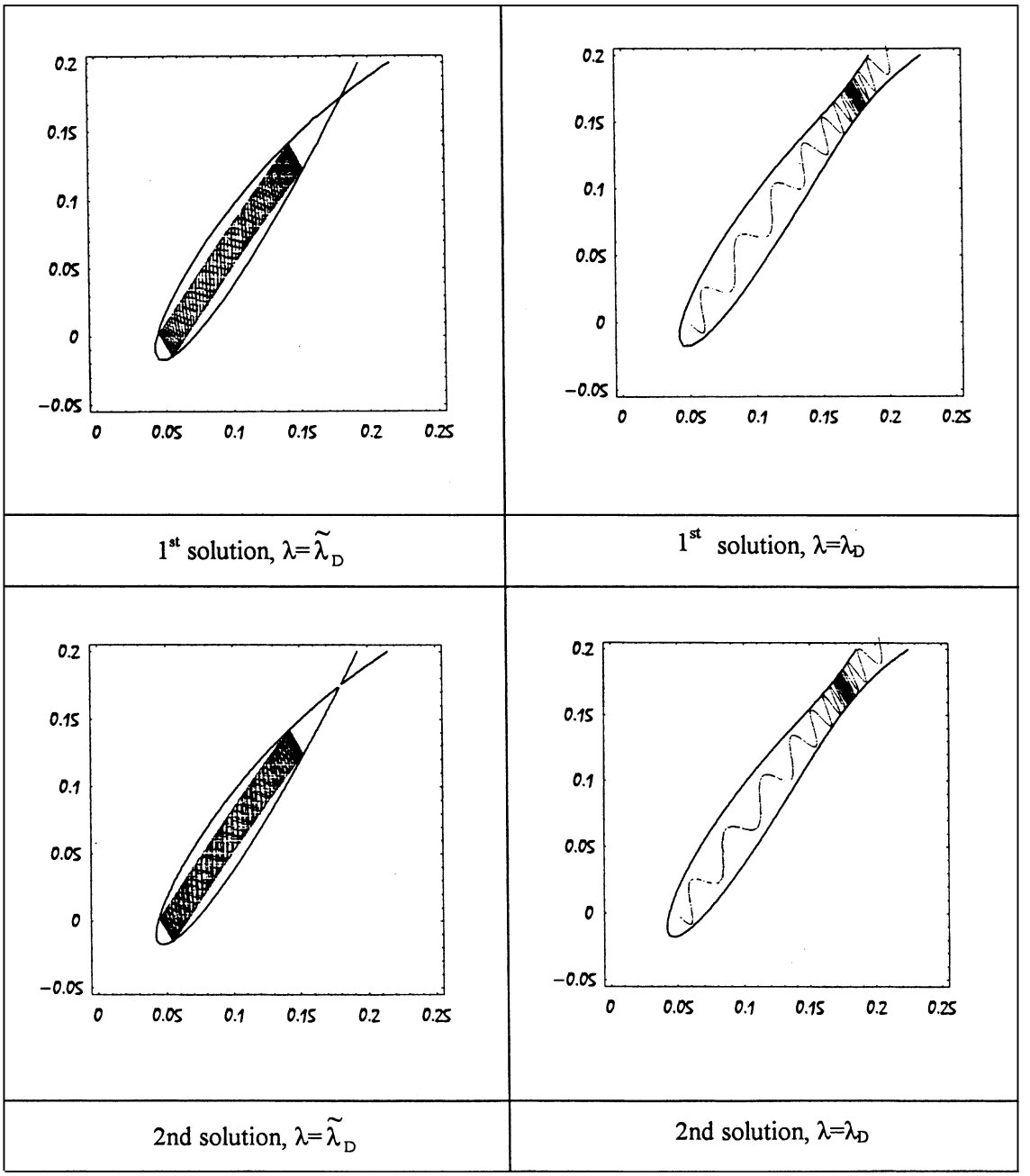

Fig. 11. Curve $\tilde{V} = 0$ and projection of motion for a 2-DOF Ziegler model with $\varepsilon_1 = 0.05$, $\varepsilon_2 = 0$, $\delta_1 = -2.5$, $\delta_2 = -0.75$, $\mu_1 = 1.8$, $\mu_0 = 0.1$, $h = 1.6$.

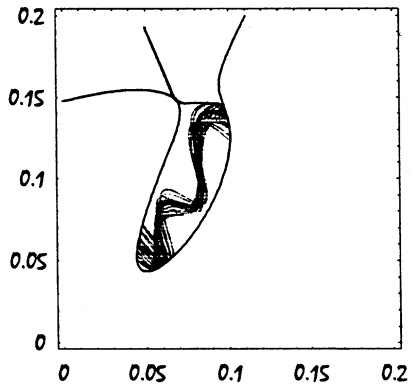

Fig. 12. Curve $\tilde{V}=0$ and projection of motion for a 2-DOF Ziegler model with $\varepsilon_1=0.05$, $\varepsilon_2=0.05$, $\delta_1=1$, $\delta_2=-10.1$, $\mu_1=1.84$, $\mu_0=0.08$, $h=2.2$.

Appendix A

For the 2-DOF nondissipative cantilever model of Ziegler shown in Fig. 9, the equations of motion (4) are simplified by linearization and omission of damping terms, and are written in matrix form as follows:

$$\begin{bmatrix} 1+m & 1 \\ 1 & 1 \end{bmatrix} \begin{Bmatrix} \ddot{\theta}_1 \\ \ddot{\theta}_2 \end{Bmatrix} + \begin{bmatrix} 2-\lambda & -1 \\ -1 & 1-\lambda \end{bmatrix} \begin{Bmatrix} \theta_1 \\ \theta_2 \end{Bmatrix} + \begin{Bmatrix} -2\varepsilon_1+\varepsilon_2 \\ \varepsilon_1-\varepsilon_2 \end{Bmatrix} = \mathbf{0} \tag{A.1}$$

which can be rearranged as:

$$\ddot{\boldsymbol{\theta}} + \mathbf{A}\cdot\boldsymbol{\theta} + \boldsymbol{\varepsilon} = \mathbf{0} \tag{A.2}$$

where

$$\boldsymbol{\theta} = \{\theta_1 \quad \theta_2\}^{\mathrm{T}}, \qquad \boldsymbol{\varepsilon} = \frac{1}{m}\begin{Bmatrix} -3\varepsilon_1+2\varepsilon_2 \\ 3\varepsilon_1-2\varepsilon_2+m(\varepsilon_1-\varepsilon_2) \end{Bmatrix} \tag{A.3}$$

$$\mathbf{A} = \frac{1}{m}\begin{bmatrix} 3-\lambda & -2+\lambda \\ -3-m+\lambda & 2+m-\lambda-m\lambda \end{bmatrix} \tag{A.4}$$

After computing the eigenfrequencies ω_1 and ω_2 and the corresponding eigenvectors $\mathbf{h}_1$ and $\mathbf{h}_2$ of matrix $\mathbf{A}$ (A.2) can be written as:

$$\ddot{\boldsymbol{\theta}} + \mathbf{H}\cdot\mathbf{D}\cdot\mathbf{H}^{-1}\cdot\boldsymbol{\theta} + \boldsymbol{\varepsilon} = \mathbf{0} \tag{A.5}$$

where

$$\mathbf{H} = [\mathbf{h_1} \quad \mathbf{h_2}], \mathbf{D} = \mathrm{diag}\{\omega_1^2, \omega_2^2\} \tag{A.6}$$

Then, by setting:

$$\mathbf{H}^{-1}\cdot\boldsymbol{\theta} = \boldsymbol{\phi} \tag{A.7}$$

we obtain two decoupled equations:

$$\begin{aligned} \ddot{\phi}_1 + \omega_1^2\phi_1 + E_1 = 0 \\ \ddot{\phi}_2 + \omega_2^2\phi_2 + E_2 = 0 \end{aligned} \tag{A.8}$$

where

$$\{ E_1 \quad E_2 \}^{\mathrm{T}} = \mathbf{H}^{-1} \cdot \boldsymbol{\varepsilon} \tag{A.9}$$

The solution of (A.8) is

$$\begin{aligned} \phi_1 &= a_1 \sin(\omega_1 t) + b_1 \cos(\omega_1 t) - \frac{E_1}{\omega_1^2} \\ \phi_2 &= a_2 \sin(\omega_2 t) + b_2 \cos(\omega_2 t) - \frac{E_2}{\omega_2^2} \end{aligned} \tag{A.10}$$

The constants a_1, a_2, b_1, b_2 are obtained from the initial conditions:

$$\begin{aligned} \{ \phi_1(0) \quad \phi_2(0) \}^{\mathrm{T}} &= \left\{ b_1 - \tfrac{E_1}{\omega_1^2} \quad b_2 - \tfrac{E_2}{\omega_2^2} \right\}^{\mathrm{T}} = H^{-1} \{ \varepsilon_1 \quad \varepsilon_2 \}^{\mathrm{T}} \\ \{ \dot{\phi}_1(0) \quad \dot{\phi}_2(0) \}^{\mathrm{T}} &= \{ a_1 \omega_1 \quad a_2 \omega_2 \}^{\mathrm{T}} = H^{-1} \{ v_1 \quad v_2 \}^{\mathrm{T}} \end{aligned} \tag{A.11}$$

where v_1 and v_2 are the known initial velocities obtained in Section 5. Then, by back transformation, we obtain:

$$\boldsymbol{\theta} = \mathbf{H} \cdot \boldsymbol{\phi} \tag{A.12}$$

Following the evaluation of $\boldsymbol{\theta}$, the direction of motion is obtained by calculating the coordinates θ_1 and θ_2 shortly after the start of motion while the calculation of the linearized amplitude requires successive iterations to detect reversal of motion.

References

Bolotin, V.V., 1964. The Dynamic Stability of Elastic Systems. Holden-Day, San Francisco, CA.

Carr, J., 1981. Applications of the Center Manifold Theorem. Springer, Berlin.

Chow, S.N., Hale, J.K., 1982. Methods of Bifurcation Theory. Springer, Berlin.

Gantes, C.J., Kounadis, A.N., 1995. Energy based dynamic buckling estimates for autonomous dissipative systems. AIAA J. 33, 1342–1349.

Gantes, C.J., Kounadis, A.N., Mallis, J., 1998. Approximate dynamic buckling loads of discrete systems via geometric considerations of their energy surface. Comput. Mech. 21, 398–402.

Goldsmith, W., 1960. IMPACT, the theory and physical behavior of colliding solids. Edward Arnold, London.

Kounadis, A.N., 1982. Impact of a body on a mass attached to an elastically restrained beam. ZAMM 62, 573–580.

Kalathas, N., Kounadis, A.N., 1991. Metastability and chaoslike phenomena in nonlinear dynamic buckling of a simple two-mass system under step load. Arch. Appl. Mech. 61, 162–179.

Kounadis, A.N., 1991a. Nonlinear dynamic buckling of discrete dissipative or non-dissipative systems under step loading. AIAA J. 29 (3), 280–289.

Kounadis, A.N., 1991b. Chaoslike phenomena in the nonlinear dynamic stability of discrete damped or undamped systems under step loading. Int. J. Non-Linear Mech. 26 (3/4), 301–311.

Kounadis, A.N., 1993a. Static and dynamic, local and global, bifurcation in nonlinear autonomous structural systems. AIAA J. 31 (8), 1468–1477.

Kounadis, A.N., 1993b. Nonlinear dynamic buckling of discrete structural systems under impact loading. Int. J. Solids Struct. 30 (21), 2895–2909.

Kounadis, A.N., 1994. A qualitative analysis for the local and global dynamic buckling and stability of autonomous discrete systems. Quartely J. Mech. Appl. Math. 47 (2), 269–295.

Kounadis, A.N., 1996a. Qualitative criteria in non-linear dynamic buckling and stability of autonomous dissipative systems. Int. J. Non-linear Mechanics 31 (6), 887–906.

Kounadis, A.N., 1996b. On the nonlinear dynamic buckling mechanism of autonomous dissipative/nondissipative discrete structural systems. Archive Appl. Mech. 66, 395–408.

Kounadis, A.N., Raftoyiannis, J., 1997. Dynamic buckling and global stability of dissipative/nondissipative systems exhibiting mode coupling under step loading. XXII Yugoslav Cong. Theor. Appl. Mech. June 2–7, Venjacka Banja, vol. of Invited Lectures, pp. 15–30.

Kounadis, A.N., Gantes, C.J., Simitses, G.J., 1997. Nonlinear dynamic buckling of multi-DOF structural dissipative systems under impact loading. Int. J. Impact Engng. 19 (1), 63–80.

Kounadis, A.N., 1998. A geometric approach for dynamic buckling of autonomous lumped-mass systems under impact. SUSI '98 International Conference, Structures under Shock and Impact, Computational Mechanics Publications, Thessaloniki, Greece, pp. 23–29.

Kounadis, A.N., Gantes, C.J., Bolotin, V.V., 1999. Dynamic buckling loads of autonomous potential systems based on the geometry of their energy surface. Int. J. Eng. Sci. 37, 1611–1628.

Kounadis, A.N., 1999a. A geometric approach for establishing dynamic buckling loads of autonomous potential lumped-mass systems. J. Appl. Mech. ASME 66 (1), 55–61.

Simitses, G., 1989. Dynamic Stability of Suddenly Loaded Structures. Springer, New York.

Thompson, J.M.T., Stewart, H.B., 1986. Nonlinear Dynamics and Chaos. Wiley, Chichester.